[Channels 3:2, 110-121; March/April 2009]; ©2009 Landes Bioscience

Research Paper

$Ca_V2.1$ P/Q-type calcium channel alternative splicing affects the functional impact of familial hemiplegic migraine mutations

Implications for calcium channelopathies

Paul J. Adams,[1] Esperanza Garcia,[1] Laurence S. David,[1] Kirk J. Mulatz,[1] Sian D. Spacey[1,2] and Terrance P. Snutch[1,*]

[1]Michael Smith Laboratories; and [2]Division of Neurology; University of British Columbia; Vancouver, BC CA

Key words: calcium channel, P/Q-type, familial hemiplegic migraine, alternative splicing

Alternative splicing is known to generate multiple functionally distinct calcium channel variants that exhibit unique spatial and temporal expression patterns. In humans, naturally occurring mutations in genes encoding calcium channel pore forming α_1-subunits are associated with several severe hereditary disorders although it remains to be described whether there exists any relationship between the physiological effects of these mutations and calcium channel splice variation. In the present study, we systematically compare the biophysical effects of three type-1 familial hemiplegic migraine (FHM-1) mutations in two predominant splice variants of the neuronal $Ca_V2.1$ P/Q-type channel. All three FHM-1 mutations cause a greater hyperpolarizing shift in voltage-dependent properties when expressed in the short carboxyl terminus variant ($Ca_V2.1$ Δ47) compared to the long variant ($Ca_V2.1$ +47). Furthermore, the FHM-1 mutations also exhibit differential splice variant-specific effects on recovery from inactivation and accumulation of inactivation during tonic and burst firing. Our findings provide important insight concerning the role of calcium channel alternatively spliced variants and the molecular pathophysiology of FHM-1 and potentially of other calcium channelopathies.

Introduction

Voltage-gated calcium channels are important in many normal physiological processes including muscle contraction, neurotransmitter release, regulation of calcium-dependent enzymes and gene expression (reviewed in ref. 1). It is therefore perhaps not surprising that naturally occurring mutations in calcium channel genes have been implicated in a number of severe human diseases. Since the first mutation in a calcium channel was identified,[2,3] over 150 individual mutations have now been reported in five of the ten genes encoding calcium channel pore forming α_1-subunits (Ca_V) and are associated with nine distinguishable disorders ("calcium channelopathies"). Over the past decade studies using recombinant channels in various expression systems have shown that many of these mutations have significant positive or negative effects on channel gating and/or expression levels, while others result in non-functional channels or have dominant negative effects (reviewed in ref. 4). It is noteworthy that the effects of mutations on channel function have thus far only been tested in a small subset of known calcium channel variants and a direct comparison of how mutations affect channel alternative splice variants has been largely unexplored.

It has been predicted that the ten genes encoding Ca_V subunits have the potential to generate thousands of functionally distinct splice variants.[5,6] Indeed, isolation and characterization of some variants has shown that alternative splicing can be a means to obtain specialized calcium channel function and to optimize calcium signalling regionally, temporally and under altered environmental conditions (reviewed in refs. 6–8). It is evident that mutations directly at a splice-site or in an alternate exon can have effects on pre-mRNA splicing and/or affect a subset of splice variants expressing alternate exons.[9-12] However, the majority of identified mutations associated with calcium channelopathies are missense mutations in coding sequences other than splice-sites and alternate exons (reviewed in ref. 4). Whether channel splice variants have different functional responses to disease-causing missense mutations has not been directly explored. We hypothesized that point mutations associated with calcium channelopathies might have splice-variant specific effects with important implications for both understanding disease pathophysiology and also towards interpreting results obtained from heterologous studies using recombinant channels.

Familial Hemiplegic Migraine (FHM) is an autosomal dominant subtype of migraine characterized by an aura of hemiplegia that is associated with at least one other aura symptom such as hemianopsia, hemisensory deficit or aphasia.[13,14] Approximately 20 missense mutations associated with FHM have been identified in the CACNA1A gene[15] (called FHM-1) which encodes the

*Correspondence to: Terrance P. Snutch; Michael Smith Laboratories; University of British Columbia; Rm 219-2185 East Mall; Vancouver, BC V6T 1Z4 CA; Tel.: 604.822.6968; Fax: 604.822.6470; Email: snutch@msl.ubc.ca

Submitted: 01/23/09; Accepted: 01/23/09

Previously published online as a *Channels* E-publication:
http://www.landesbioscience.com/journals/channels/article/7932

α_1 subunit ($Ca_V2.1$; α_{1A}) of the P/Q-type voltage-gated calcium channel. P/Q-type calcium channels are abundantly expressed throughout mammalian brain and spinal cord where they mediate calcium influx essential for neurotransmitter release, calcium-mediated second messenger signalling and calcium-dependent gene transcription.[16-20] The functional consequences of FHM-1 mutations on $Ca_V2.1$ P/Q-type channel properties have been investigated in heterologous *Xenopus* oocyte and mammalian expression systems, and more recently in neurons and whole brains of FHM-1 mutant R192Q and S218L knock-in mice.[21-28] While there have been some noted discrepancies reported, in both heterologous and knock-in mice systems there is a general demonstrated trend for FHM-1 mutations to exhibit gain-of-function properties: increased channel availability and increased calcium influx at lower membrane potentials resulting in a greater susceptibility to the cortical spreading depression (CSD) thought to be the underlying mechanism of aura.[21,22,27,29-31]

There are seven identified alternatively spliced sites within the $Ca_V2.1$ subunit gene and the various splice variants exhibit distinct biophysical characteristics, calcium-dependent properties, pharmacological sensitivities and subtype-specific temporal and regional localizations in human brain.[16,32-35] However, it is not known whether the functional impact of FHM-1 mutations is similar amongst the different $Ca_V2.1$ splice variants or whether alternative splicing contributes to the spatial and temporal nature of the FHM-1 phenotype. The carboxyl terminus of $Ca_V2.1$ channels is known to affect several physiological processes and alternative splicing in this region confers functional changes in channel properties.[16,32,35-38] The most substantial changes induced by alternative splicing in the C-terminus of $Ca_V2.1$ channels results from the use of an alternative three prime acceptor site in the intron upstream of the last exon, exon 47.[32,36,39,40] Alternative splicing at exon 47 introduces a frame-shift resulting in a stop codon at the beginning of exon 47. As a result, P/Q-type channels can be of either the short form (isoform 1; $Ca_V2.1$ (Δ47)) or the long form (isoform 2; $Ca_V2.1$ (+47)). The voltage-dependent and kinetic properties of the $Ca_V2.1$ (+47) and $Ca_V2.1$ (Δ47) splice variants and their relative contributions concerning FHM-1 mutations has not been explored.

In the present study we compared the biophysical properties of wild-type (WT) $Ca_V2.1$ (+47) and $Ca_V2.1$ (Δ47) P/Q-type channel splice variants and also explored the effects of three FHM-1 mutations introduced into the two variants. We investigated two mutations, K1336E and R192Q, that are associated with an FHM-1 phenotype of pure hemiplegia and migraine without any other neurological symptoms.[14,15] We further investigated the S218L FHM-1 mutation which is associated with a severe clinical phenotype wherein typical FHM-1 attacks induced by minor head trauma are often followed by a delayed cerebral edema, fever, stupor and sometimes coma (fatal in one reported instance).[41-43] We find that the two P/Q-type channel carboxyl tail splice variants exhibit functionally distinct properties and also that the three FHM-1 mutations have differential splice-dependent effects on voltage-dependent and kinetic properties. We discuss the potential importance of the splice-variant differential effects in the context of FHM-1 pathophysiology as well as the implications for other calcium channelopathies.

Results

$Ca_V2.1$ (+47) and $Ca_V2.1$ (Δ47) variants are expressed in human cortex. Mutations in the P/Q-type channel $Ca_V2.1$ subunit underlie FHM-1 and the current consensus is that initiation of migraine attacks is in the cortex, however the expression of splice variants has not yet been described in the human cortex . In order to determine whether the $Ca_V2.1$ (+47) and $Ca_V2.1$ (Δ47) variants are expressed in human cortex we utilized RT-PCR to amplify a ~1.1 Kb carboxyl terminal fragment of $Ca_V2.1$ from adult human cortex RNA using oligonucleotide primers that recognize both carboxyl alternatively spliced variants in a non-biased manner. The PCR products were subsequently re-amplified using splice-variant specific primers. Figure 1 shows that the $Ca_V2.1$ (+47) and $Ca_V2.1$ (Δ47) splice variants are both expressed in human cortex. To determine their relative proportions, the human cortical $Ca_V2.1$ carboxyl terminal PCR products were sub-cloned and individual cDNAs analyzed using splice-variant specific primers and direct DNA sequencing. From the 53 cDNA clones analyzed we determined that the $Ca_V2.1$ (+47) and $Ca_V2.1$ (Δ47) splice variants were present in whole cortex in relative proportions of 79% and 21%, respectively.

All subsequent biophysical analyses were performed using human long $Ca_V2.1$ (+47) and short $Ca_V2.1$ (Δ47) splice-variant cDNA clones with either WT or FHM-1 mutant K1336E, R192Q or S218L changes introduced (see Fig. 1A for the location of the FHM-1 mutations).

FHM-1 mutations exhibit differential effects on the voltage-dependent properties of $Ca_V2.1$ splice variants. Whole cell current analysis of transiently transfected cells showed that the WT $Ca_V2.1$ (Δ47) and WT $Ca_V2.1$ (+47) variants possess similar membrane potentials at which half the channels are activated (V_{50act} = -14.02 ± 1.49, and -15.08 ± 1.20, respectively) and similar membrane potentials at which half of the channels are inactivated ($V_{50inact}$ = -58.20 ± 2.04, and -62.07 ± 1.87, respectively; see Table 1 and Fig. 2). The K1336E, R192Q and S218L mutations have been previously reported to cause a hyperpolarizing shift in the current-voltage relationship relative to WT $Ca_V2.1$ channels.[24,26,27,29,46] Examining the FHM-1 mutations in the P/Q-type +47 and Δ47 carboxyl tail splice variants we found differential effects. The K1336E $Ca_V2.1$ (+47) and R192Q $Ca_V2.1$ (+47) channels both exhibited a small but significant shift in V_{50act} relative to WT $Ca_V2.1$ (+47) channels (-21.53 ± 1.35 and -19.11 ± 1.11 vs. -15.08 ± 1.20, respectively; $p < 0.05$; ANOVA), while the S218L mutation had no significant affect on $Ca_V2.1$ (+47) channels relative to WT (Table 1 and Fig. 2). In contrast, all three FHM-1 mutations caused large significant hyperpolarizing shifts in V_{50act} when expressed in $Ca_v2.1$ (Δ47) variant channels ($p < 0.001$; ANOVA; Table 1 and Fig. 2). Similar differential splice-dependent effects of the FHM-1 mutations were apparent in examining $V_{50inact}$. Figure 2 shows that the R192Q and S218L mutations resulted in large (~15–17 mV) hyperpolarizing shifts in $V_{50inact}$ in the $Ca_V2.1$ (Δ47) variant relative to WT $Ca_V2.1$ (Δ47) channels ($p < 0.001$; ANOVA), while

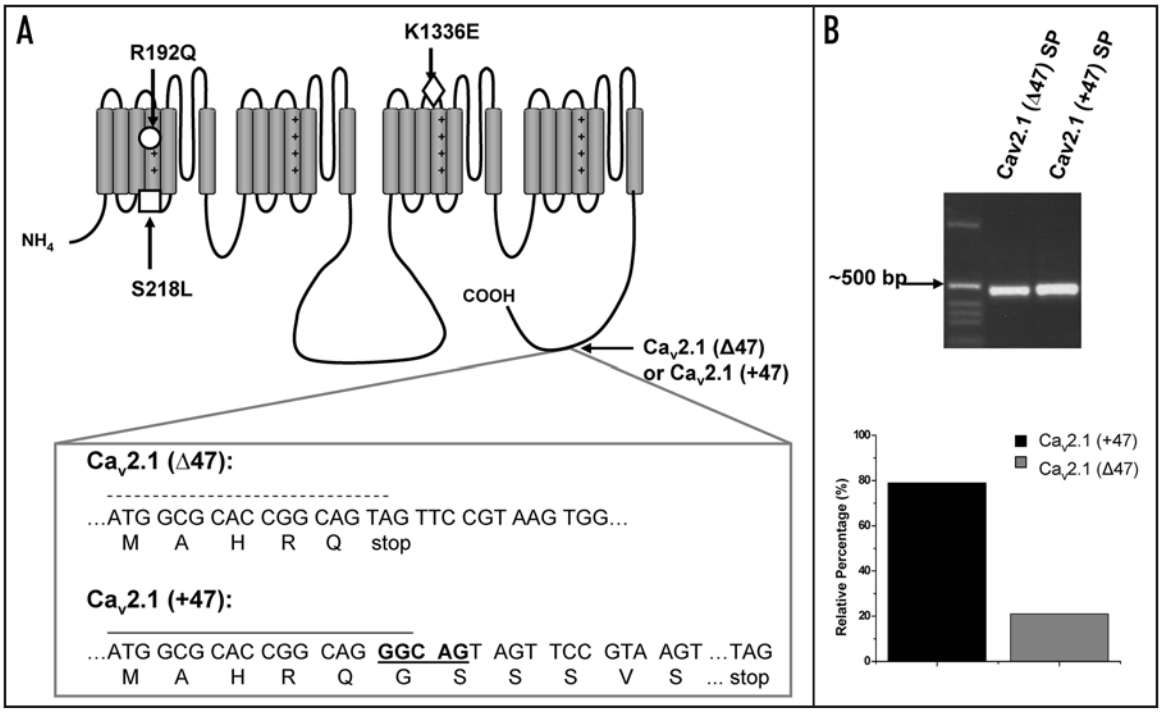

Figure 1. Human P/Q-type calcium channel topology and splice-variant expression in human cortex. (A) schematic showing the location of the three FHM-1 mutations and the carboxyl terminal splice site in the human $Ca_V2.1$ channel. In the box below the channel diagram are partial sequences of the $Ca_V2.1$ (+47) and $Ca_V2.1$ (Δ47) variants at the exon 46/exon 47 boundary. The pentanucleotide insertion is shown in bold for the $Ca_V2.1$ (+47) variant. (B) the last ~1 Kb of the $Ca_V2.1$ carboxyl terminus was amplified from human cortical RNA and purified. Subsequently, splice-variant specific forward primers (SP) designed to exclusively bind either $Ca_V2.1$ (Δ47) or $Ca_V2.1$ (+47) transcripts were used in PCR reactions to generate an ~500 bp fragment from the purified carboxyl fragments; $Ca_V2.1$ (Δ47)-SP and $Ca_V2.1$ (+47)-SP, respectively (dotted line is above the sequence that $Ca_V2.1$ (Δ47)-SP binds and the solid line is above the sequence that $Ca_V2.1$ (+47)-SP binds in (A). Both splice-variant specific primers generated the expected product from the carboxyl PCR fragment of the $Ca_V2.1$ cDNA obtained from human cortex, verifying both $Ca_V2.1$ (Δ47) or $Ca_V2.1$ (+47) are present in human cortex. Products were verified by direct DNA sequencing and determined to be in relative proportions of 79% $Ca_V2.1$ (+47) and 21% $Ca_V2.1$ (Δ47) (bar graph); for protocol details see Materials and Methods.

these same two FHM-1 mutations had a smaller effects on $Ca_V2.1$ (+47) variant channels ($p < 0.05$; ANOVA; Table 1). Interestingly, the K1336E mutation did not cause a significant change in $V_{50inact}$ in either splice variant. Overall, these data indicate that the impact of individual FHM-1 mutations on P/Q-type channel gating properties is differentially affected by the nature of the splice-variant background in which the mutation is expressed.

FHM-1 mutations exhibit differential effects on recovery from inactivation of $Ca_V2.1$ splice variants. Analysis of WT $Ca_V2.1$ (Δ47) and $Ca_V2.1$ (+47) variants showed different rates of recovery from inactivation for these P/Q-type channel splice variants. WT $Ca_V2.1$ (Δ47) channels exhibit faster rates of recovery (τ_1 = 0.67 ± 0.11 and τ_2 = 3.08 ± 0.61) than the $Ca_V2.1$ (+47) variant channels (τ_1 = 0.76 ± 0.21 and τ_2 = 3.39 ± 0.84). As a result, $Ca_V2.1$ (Δ47) channels show a significantly higher percentage of channels recovered at 7.5 seconds after inactivation relative to $Ca_V2.1$ (+47) channels (89.0 ± 1.8 vs. 77.3 ± 3.8 %, respectively; $p < 0.05$; ANOVA) (Fig. 3 and Table 2).

Examining the effects of FHM-1 mutations in the $Ca_V2.1$ (Δ47) background, Figure 3 shows that the K1336E $Ca_V2.1$ (Δ47) and R192Q $Ca_V2.1$ (Δ47) variants exhibit a significant decrease in current recovered at 7.5 seconds relative to WT $Ca_V2.1$ (Δ47) channels (70.4 ± 3.7% and 83.3 ± 2.3% vs. 89.0 ± 1.8 %, respectively; $p < 0.05$; ANOVA). Contrastingly, K1336E $Ca_V2.1$ (+47) and R192Q $Ca_V2.1$ (+47) channels showed increases in recovery relative to WT $Ca_V2.1$ (+47) channels (86.8 ± 1.7 and 87.0 ± 2.0 vs. 77.3 ± 3.8 %, respectively; $p < 0.05$; ANOVA) (Fig. 3 and Table 2). The S218L mutation was found to increase the recovery in both splice variants, however, only the S218L $Ca_V2.1$ (+47) channels showed a significant increase in recovery relative to WT $Ca_V2.1$ (+47) channels at 7.5 seconds (94.7 ± 1.5 vs. 77.3 ± 3.8 %, respectively; $p < 0.001$; ANOVA) (Fig. 3 and Table 2).

Overall, in agreement with previous reports,[24,27] we observed that both the K1336E and S218L mutations can cause significant changes to recovery from inactivation and show for the first time that the R192Q mutation also changes recovery from inactivation. Importantly, we also show that the quantitative effects of the FHM-1 mutations on channel function are dependant upon the nature of the $Ca_V2.1$ splice variant. We also note that the differential effects of the mutations resulted in significant changes to the functional distinction observed between the two WT channel variants; that is, while the WT $Ca_V2.1$ (Δ47) channel variant recovered significantly faster than the WT $Ca_V2.1$ (+47) channel variant, the K1336E $Ca_V2.1$ (Δ47) channels recovered significantly slower

Table 1 **Mean values for voltage-dependent activation and inactivation parameters**

	V_{50} Activation (mV)	k Activation	τ_{act} (msec)	V_{50} Inactivation (mV)	k Inactivation
$Ca_V2.1$ (Δ47) Wild-type	-14.02 ± 1.49 (n = 16)	4.82 ± 0.27	1.42 ± 0.09	-58.20 ± 2.04 (n = 21)	7.03 ± 0.29
$Ca_V2.1$ (Δ47) K1336E	-24.12 ± 1.33# (n = 10)	2.80 ± 0.20#	1.16 ± 0.21	-62.27 ± 1.81 (n = 7)	7.23 ± 0.45
$Ca_V2.1$ (Δ47) R192Q	-20.84 ± 0.94# (n = 16)	4.30 ± 0.19	1.31 ± 0.07	-73.41 ± 3.15# (n = 11)	7.58 ± 0.57
$Ca_V2.1$ (Δ47) S218L	-24.10 ± 1.15# (n = 9)	5.53 ± 0.39	0.97 ± 0.11*	-75.07 ± 3.96# (n = 10)	6.34 ± 0.62
$Ca_V2.1$ (+47) Wild-type	-15.08 ± 1.20 (n = 16)	4.33 ± 0.24	1.28 ± 0.07	-62.07 ± 1.87 (n = 16)	6.85 ± 0.38
$Ca_V2.1$ (+47) K1336E	-21.53 ± 1.35* (n = 9)	3.10 ± 0.18*	1.33 ± 0.10	-65.02 ± 1.87 (n = 8)	8.39 ± 0.78
$Ca_V2.1$ (+47) R192Q	-19.11 ± 1.11* (n = 16)	4.79 ± 0.26	1.43 ± 0.10	-70.27 ± 2.36* (n = 16)	7.19 ± 0.47
$Ca_V2.1$ (+47) S218L	-18.08 ± 1.28 (n = 11)	6.26 ± 0.31#	1.06 ± 0.08*	-72.54 ± 1.70* (n = 9)	5.92 ± 0.37

The voltage at which half of the channels are in the activated state (V_{50act}) and inactivated state ($V_{50inact}$), and the steepness of the curves for activation (k_{act}) and inactivation (k_{inact}) were obtained by fitting the data with the Boltzmann equation for the indicated number of cells in parentheses. The kinetics of activation (τ_{act})were obtained by fitting the maximum current trace from the IV curves with a single exponential. Asterisks (*) and number signs (#) indicate significant difference relative to wild-type with p-values less than either 0.05 or 0.001 (one-way ANOVA), respectively.

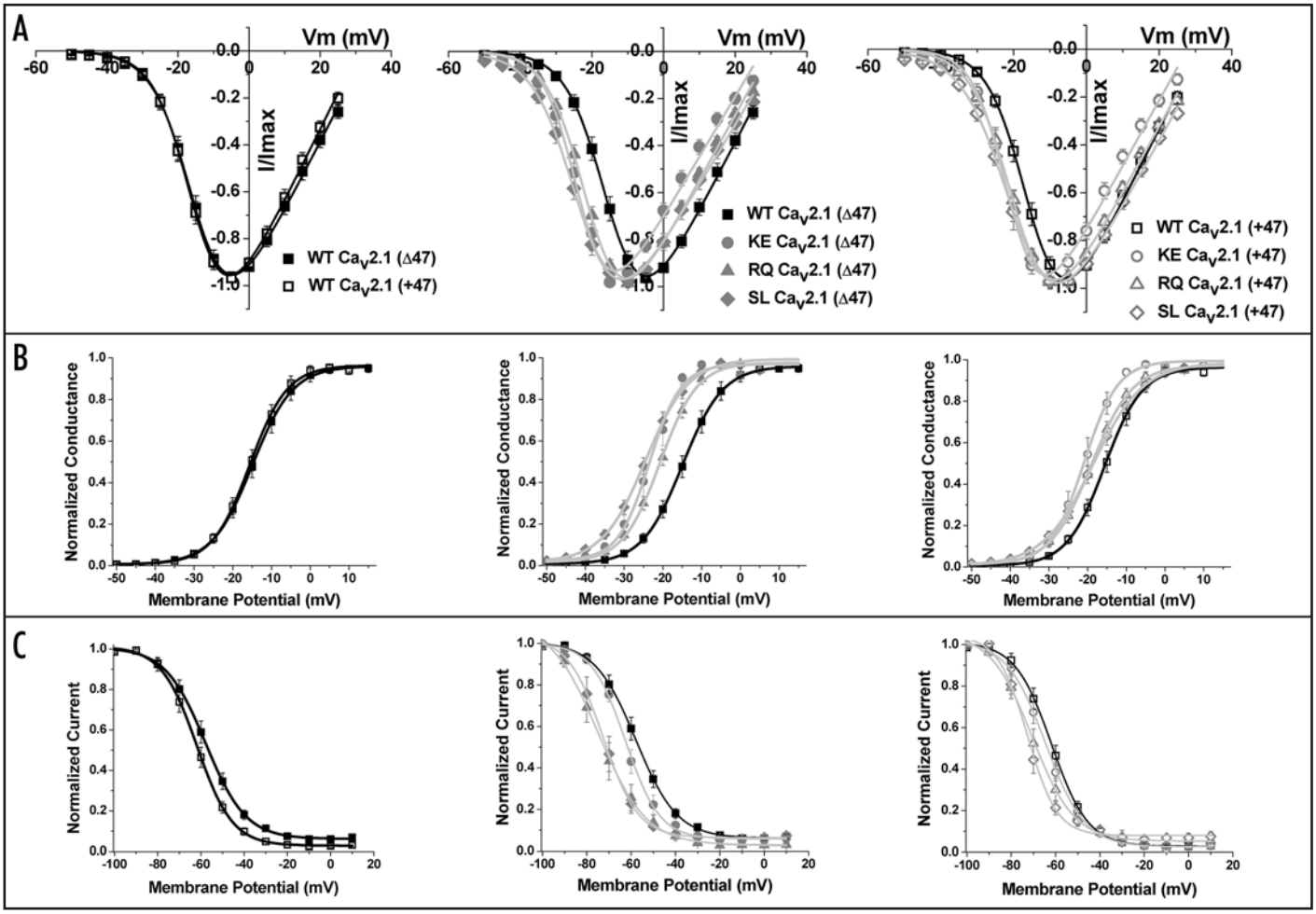

Figure 2. FHM-1 mutations differentially affect voltage-dependent properties of $Ca_V2.1$ (Δ47) and $Ca_V2.1$ (+47) P/Q-type variants. (A) shows the comparison between current-voltage relationships (IV-curves) for wild-type (WT; black squares), FHM-1 mutant K1336E (KE; grey circles), R192Q (RQ; grey triangles) and S218L (SL; grey diamond) in both the short $Ca_V2.1$ (Δ47) (filled symbols) and long $Ca_V2.1$ (+47) (open symbols) C-terminus splice variants. IV curves for all constructs were determined from currents evoked during 90 ms square pulse depolarizations shown between -50 mV and +20 mV from a holding potential of -90 mV. (B) conductance values were calculated from IV curves to obtain activation curves. (C) steady-state inactivation curves were generated using a standard protocol in which 5 s prepulse holdings of -100 to +10 mV were elicited prior to the 80 ms, 0 mV test pulse from a holding of -120 mV. Normalized current evoked during the test pulse is plotted vs. prepulse membrane potential. For complete statistics see Table 1 and for details of protocols see Methods.

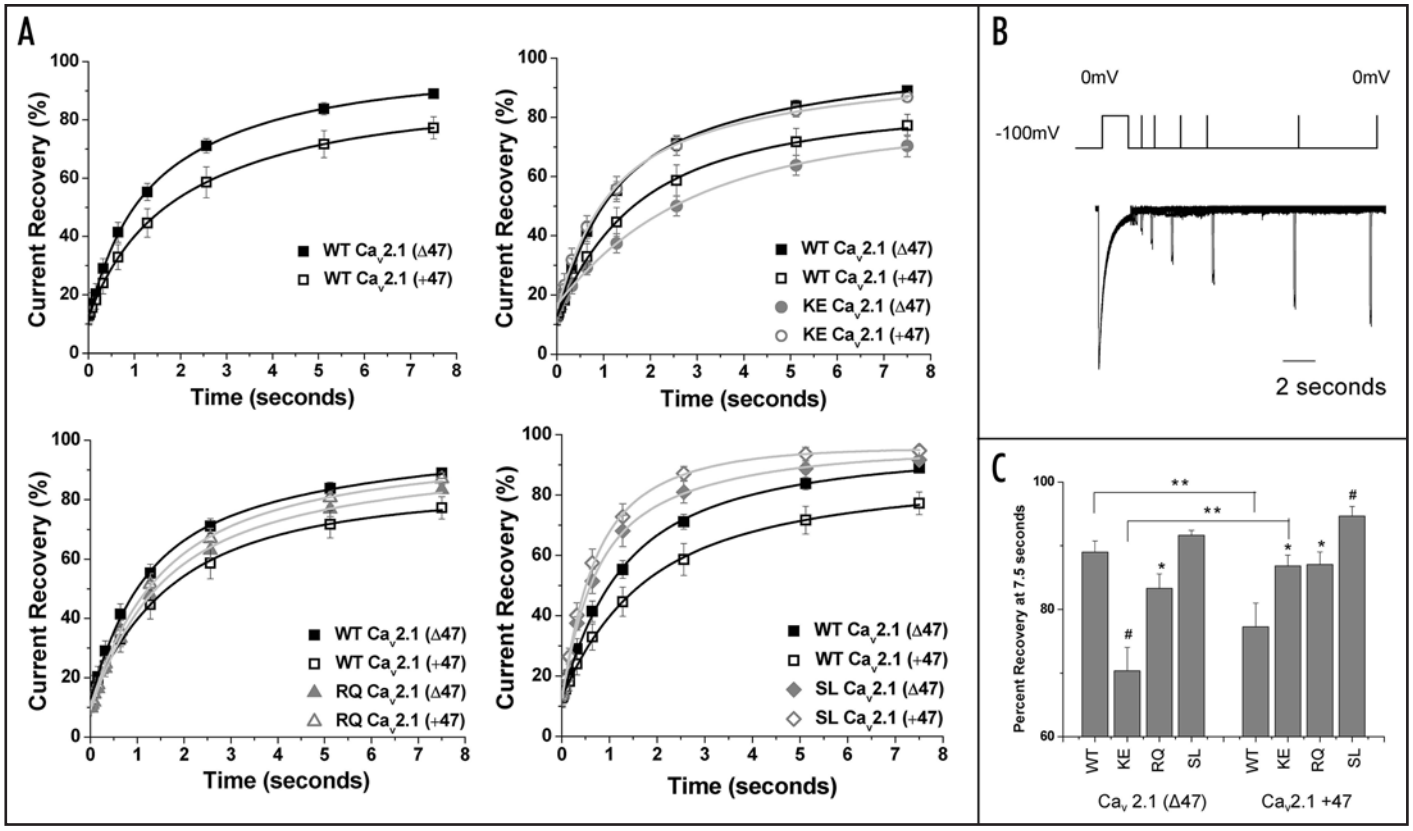

Figure 3. Wild-type and FHM-1 mutant $Ca_V2.1$ (Δ47) and $Ca_V2.1$ (+47) variants exhibit different rates of recovery from inactivation. (A) graphs show percentage of the current recovered vs. time given to recover for all WT and FHM-1 mutated constructs. Recovery from inactivation was examined for wild-type (WT; black squares), FHM-1 mutant K1336E (KE; grey circles), R192Q (RQ; grey triangles) and S218L (SL; grey diamond) in both the short $Ca_V2.1$ (Δ47) (filled symbols) and long $Ca_V2.1$ (+47) (open symbols) C-terminus splice variants. (B) shows a representative (WT) trace (transient currents removed for clarity) and the two pulse protocol used. The protocol consists of a 2 second, 0 mV prepulse followed by a 50 ms, 0 mV test pulse elicited after inter-pulse intervals between 10 ms and 7.5 seconds. Time constants were determined by fitting the average values for percent recovery with a single exponential or double exponential (values shown in Table 2). (C) bar graph shows percent recovery at 7.5 seconds for all WT and FHM-1 mutant clones studied. Single asterisks and number signs indicate significant difference between mutant and wild-type of the same variant with p-values less than either 0.05 or 0.001 (one-way ANOVA), respectively. Double asterisks indicate significant difference between the Δ47 and +47 variants containing the same sequence (i.e., WT or mutant) with p-value less than 0.05 (one-way ANOVA).

than K1336E $Ca_V2.1$ (+47) channels. In addition, the R192Q and S218L mutations altered recovery such that the R192Q $Ca_V2.1$ (Δ47) and R192Q $Ca_V2.1$ (+47) channels and S218L $Ca_V2.1$ (Δ47) and S218L $Ca_V2.1$ (+47) channels were not functionally distinct in this parameter (Fig. 3 and Table 2).

FHM-1 mutations exhibit differential effects on inactivation of $Ca_V2.1$ splice variants during tonic depolarization. WT $Ca_V2.1$ (+47) and $Ca_V2.1$ (Δ47) variants exhibit functional differences with regard to accumulation of inactivation during short (3.5 msec) 25 Hz repetitive stimulations (Fig. 4). While $Ca_V2.1$ (Δ47) variant channels showed 95.0 ± 1.4% of current remaining at the end of 25 pulses, $Ca_V2.1$ (+47) variant channels had 90.0 ± 0.9% ($p < 0.05$; ANOVA) (Fig. 4C).

All three FHM-1 mutations examined significantly altered accumulation of inactivation (Fig. 4A); however, again the effects were contingent on the nature of the $Ca_V2.1$ variant in which mutations were expressed. The K1336E $Ca_V2.1$ (Δ47) and K1336E $Ca_V2.1$ (+47) channels had a significant increase in accumulation of inactivation and thus a lower percent of current remaining at the end of 25 pulses relative to WT $Ca_V2.1$ (Δ47) and WT $Ca_V2.1$ (+47) (88.0 ± 2.2% and 84.0 ± 1.7% vs. 95.0 ± 1.4 and 90.0 ± 0.9%, respectively; $p < 0.05$; ANOVA) (Fig. 4C). The changes were such that the K1336E $Ca_V2.1$ (+47) and K1336E $Ca_V2.1$ (Δ47) variants had similar current remaining at the end of the repetitive stimulation and thus lacked the clear functional distinction observed between the WT channel variants.

In the context of the $Ca_V2.1$ (Δ47) variant background the R192Q mutation caused a significant increase in accumulation of inactivation relative to WT $Ca_V2.1$ (Δ47) (current remaining at end of the 25 pulses = 90.0 ± 1.6% vs. 95.0 ± 1.4%: $p < 0.05$; ANOVA). In contrast, R192Q $Ca_V2.1$ (+47) channels were similar to WT $Ca_V2.1$ (+47) channels (92 ± 1.3% vs. 90 ± 0.9%) (Fig. 4C). Similar to K1336E channels, the R192Q $Ca_V2.1$ (Δ47) and R192Q $Ca_V2.1$ (+47) channel variants lacked the clear functional distinction observed between the WT variants for this property.

The S218L mutation showed a large and significant increase in accumulation of inactivation and thus a lower percent of current remaining at the end of 25 pulses relative to both the WT $Ca_V2.1$ (Δ47) and $Ca_V2.1$ (+47) channel variants (81 ± 2.5% and 77 ± 1.7% vs. 95 ± 1.4 and 90 ± 0.9%, respectively; $p < 0.05$; ANOVA). Similar to that for R192Q and K1336E, a further overall effect of the S218L mutation is to decrease the relative difference in current remaining observed between WT $Ca_V2.1$ (Δ47) and $Ca_V2.1$ (+47) variant channels.

FHM-1 mutations exhibit differential effects on inactivation of $Ca_V2.1$ splice variants during bursts of depolarization. In addition to tonic depolarizations, neurons experience various frequencies of burst firing in which brief periods of tonic firing are interspersed with silent periods as the membrane potential drops below threshold.[47-51] During the tonic firing periods P/Q-type channels will inactivate and during silent periods they will have the opportunity to recover from inactivation. Based upon the above noted splice-variant changes in accumulation of inactivation and recovery from inactivation, we predicted that bursts of depolarization would also differentially affect WT and FHM-1 mutated $Ca_V2.1$ (+47) and $Ca_V2.1$ (Δ47) variant channels.

Figure 5 shows that WT $Ca_V2.1$ (+47) and $Ca_V2.1$ (Δ47) variants exhibit significant differences in the amount of current remaining at the end of five 25 Hz bursts given at 3.5 Hz. Current through the WT $Ca_V2.1$ (+47) variant decayed to 73 ± 3.4% by the end of the fifth burst while current through the WT $Ca_V2.1$ (Δ47) variant decayed to 88 ± 3.6% ($p < 0.05$; ANOVA) (Fig. 5C). The increased inactivation during the depolarizations and the reduced recovery from inactivation of WT $Ca_V2.1$ (+47) variants discussed above likely contributed to the overall 15% decrease in current relative to the WT $Ca_V2.1$ (Δ47) variant.

Figure 5 shows that during burst firing the K1336E mutation in the $Ca_V2.1$ (Δ47) variant background results in an overall lower percentage of current remaining at the end of five bursts (70 ± 4.9% vs. 88 ± 3.6%, respectively; $p < 0.05$; ANOVA) (Fig. 5C), likely resulting from the increased accumulation of inactivation and slowed recovery from inactivation of K1336E $Ca_V2.1$ (Δ47) channels relative to WT $Ca_V2.1$ (Δ47) (see Figs. 3 and 4). Contrastingly, the K1336E mutation in the $Ca_V2.1$ (+47) variant background did not show significant current decay relative to WT, likely due to the fact that although the K1336E $Ca_V2.1$ (+47) variant channels exhibit a small increase in accumulation of inactivation during tonic stimulation (Fig. 4), they also possess an increased rate of recovery from inactivation (Fig. 3A). We note that unlike WT channel variants, the K1336E $Ca_V2.1$ (+47) and K1336E $Ca_V2.1$ (Δ47) variants did not differ significantly relative to one another.

Similar to that for the K1336E mutation in the Δ47 background, examination of burst firing effects on the R192Q mutation showed an increase in current decay during burst firing relative to WT $Ca_V2.1$ (Δ47) channels (70 ± 3.6% vs. 88 ± 3.6% current remaining, respectively; $p < 0.05$; ANOVA) (Fig. 5C). In contrast, the R192Q mutation in the +47 background resulted in a higher degree of current remaining compared to WT $Ca_V2.1$ (+47) channels (83 ± 2.7% vs. 73 ± 3.4% current remaining, respectively; $p < 0.05$; ANOVA). This may reflect the fact that R192Q $Ca_V2.1$ (+47) channels exhibit increased recovery from inactivation (see Fig. 3). We note that an overall effect concerning current decay during burst firing is for R192Q $Ca_V2.1$ (+47) channels to behave more similar to that for the WT Δ47 channels and for R192Q $Ca_V2.1$ (Δ47) channels to behave more similar to those of the WT +47 variant.

Similar to that for the K1336E mutation, the S218L mutation only caused a significant current decay during the burst firing in the $Ca_V2.1$ (Δ47) variant background (73.0 ± 4.0% vs. 88.0 ± 3.6% current remaining at the end of five bursts, respectively; $p < 0.05$; ANOVA). Presumably, although the S218L mutation increased accumulation of inactivation substantially in both splice variants (see Fig. 4), S218L $Ca_V2.1$ (+47) channels had a larger increase in the rate of recovery from inactivation (Fig. 3) which likely slowed overall accumulation of inactivation during the burst firing. The S218L $Ca_V2.1$ (+47) and S218L $Ca_V2.1$ (Δ47) variants did not differ significantly relative to one another.

Table 2 Time constant values and recovery from inactivation

	τ_1 (Fast) (msec)	τ_2 (Slow) (msec)	% Recovery at 7.5 seconds
$Ca_V2.1$ (Δ47) Wild-type	0.67 ± 0.11	3.08 ± 0.61	89.0 ± 1.8 (n = 5)
$Ca_V2.1$ (Δ47) K1336E	2.89 ± 0.12	N.A.	70.4 ± 3.7# (n = 8)
$Ca_V2.1$ (Δ47) R192Q	0.91 ± 0.19	4.97 ± 2.65	83.3 ± 2.3* (n = 7)
$Ca_V2.1$ (Δ47) S218L	0.617 ± 0.10	2.71 ± 1.18	91.6 ± 0.8 (n = 5)
$Ca_V2.1$ (+47) Wild-type	0.76 ± 0.21	3.39 ± 0.84	77.3 ± 3.8** (n = 7)
$Ca_V2.1$ (+47) K1336E	0.54 ± 0.13	2.67 ± 0.53	86.8 ± 1.7* (n = 5)
$Ca_V2.1$ (+47) R192Q	1.08 ± 0.20	5.78 ± 4.96	87.0 ± 2.0* (n = 6)
$Ca_V2.1$ (+47) S218L	0.50 ± 0.12	1.71 ± 0.59	94.7 ± 1.5# (n = 5)

Time constants were determined by fitting the average percent recovery with a double exponential for all constructs except the $Ca_V2.1$ (Δ47) K1336E which was best fit with a single exponential. Percent recovery is a measure of the percentage of current evoked during the test pulse, given at 7.5 seconds after the prepulse, relative to the maximum current evoked during the prepulse. Asterisks and number signs indicate significant difference between mutant and wild-type of the same variant with p-values less than either 0.05 or 0.001 (one-way ANOVA), respectively. Double asterisks indicate significant difference between the $Ca_V2.1$ Δ47 and +47 variants containing the same sequence (i.e. WT or mutant) with p-value less than 0.05 (one-way ANOVA). Number of cells recorded for each clone is indicated in parenthesis. N.A. = not applicable.

Discussion

We report here that FHM-1 missense mutations confer differential effects on the biophysical properties of the $Ca_V2.1$ (+47) and $Ca_V2.1$ (Δ47) P/Q-type channel splice variants. Although the current-voltage relationships and steady-state properties of the two WT P/Q-type splice variants are similar, all three

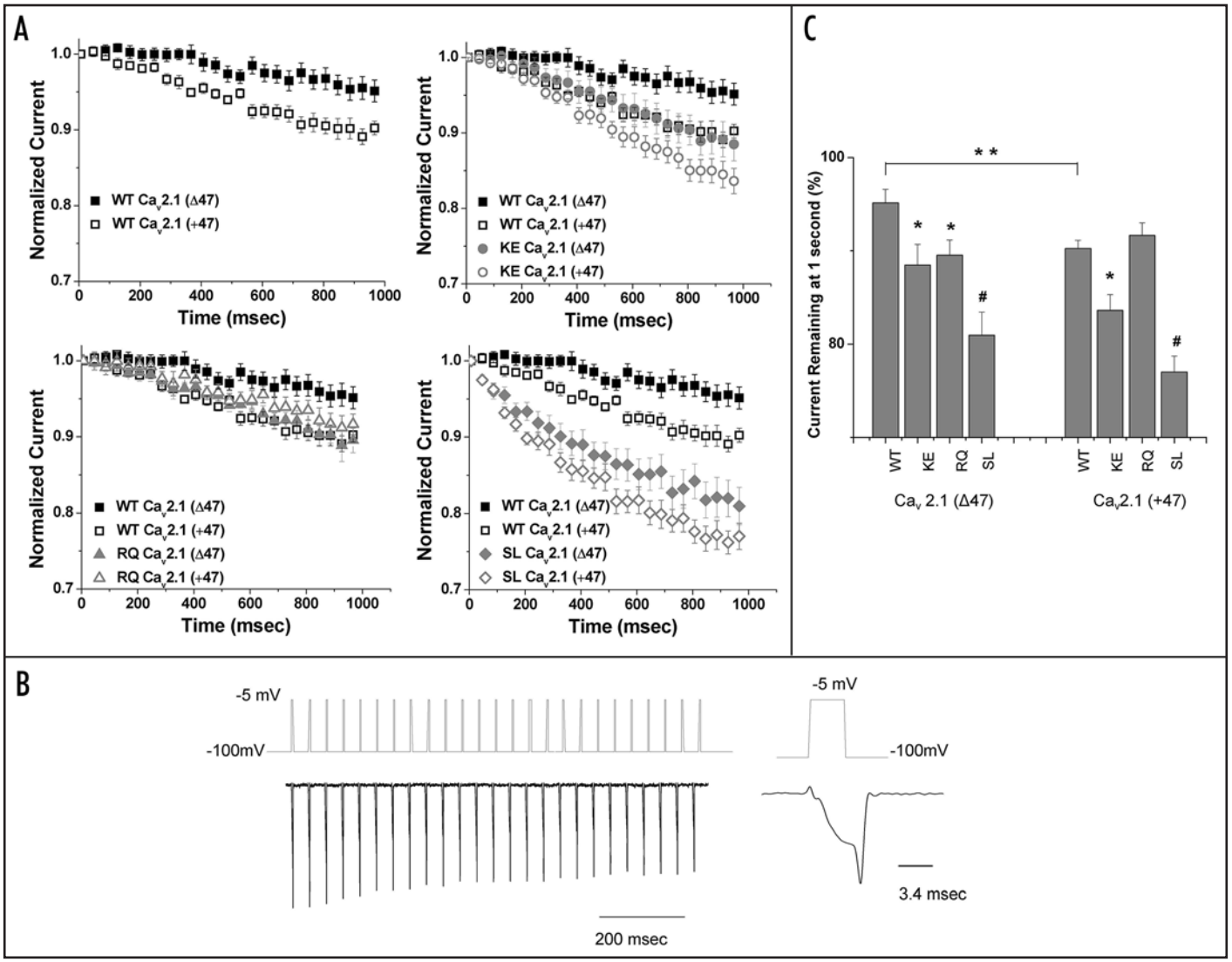

Figure 4. Wild-type and FHM-1 mutant $Ca_V2.1$ (Δ47) and $Ca_V2.1$ (+47) variants exhibit different current decay during 25 Hz tonic depolarizations. (A) graphs show normalized current remaining vs. time after initial onset of depolarizations. Current decay was measured for wild-type (WT; black squares), FHM-1 mutant K1336E (KE; grey circles), R192Q (RQ; grey triangles) and S218L (SL; grey diamond) in both the short $Ca_V2.1$ (Δ47) (filled symbols) and long $Ca_V2.1$ (+47) (open symbols) C-terminus splice variants. (B) to investigate current decay during repetitive stimulations we used 25 square pulses from a holding of -100 mV to a depolarizing potential of -5 mV for a duration of 3.4 ms. The test pulses were given at a rate of 25 Hz. Representative current trace and pulse protocol indicated at bottom (capacitive transients were compensated using a P/4 protocol), with single current response enlarged. (C) bar graph shows the percent of current remaining at the end of 25 pulses for each clone. Single asterisks and number signs indicate significant difference between mutant and wild-type of the same variant with p-values less than either 0.05 or 0.001 (one-way ANOVA), respectively. Double asterisks indicate significant difference between the Δ47 and +47 variants containing the same sequence (i.e., WT or mutant) with p-value less than 0.05 (one-way ANOVA). Number of cells recorded for WT $Ca_V2.1$ (Δ47) (n = 14), WT $Ca_V2.1$ (+47) (n = 13), KE $Ca_V2.1$ (Δ47) (n = 15), KE $Ca_V2.1$ (+47) (n = 18), RQ $Ca_V2.1$ (Δ47) (n = 17), RQ $Ca_V2.1$ (+47) (n = 15), SL $Ca_V2.1$ (Δ47) (n =15), SL $Ca_V2.1$ (+47) (n = 14).

FHM-1 mutations exhibited a greater hyperpolarizing shift when expressed in the $Ca_V2.1$ (Δ47) variant compared to the $Ca_V2.1$ (+47) variant (Fig. 2). In addition, we show for the first time that WT $Ca_V2.1$ (Δ47) and WT $Ca_V2.1$ (+47) variants have both different kinetics of recovery from inactivation and accumulation of inactivation during tonic depolarization that are likely relevant to the differential response of channel variants during bursts of depolarization (Figs. 3–5). It is known that $Ca_V2.1$ channels in different states possess alternative modes of gating that are reflected in biophysical properties at the whole cell current level.[52,53] Furthermore, it has been shown that alternative splicing in the EF-hand region of the $Ca_V2.1$ carboxyl terminus can shift gating modes.[54] It is therefore possible that WT $Ca_V2.1$ (Δ47) and WT $Ca_V2.1$ (+47) variants also have distinct gating modes that respond differently to FHM-1 mutations which are localized near voltage sensor regions (e.g., R192Q, S218L,

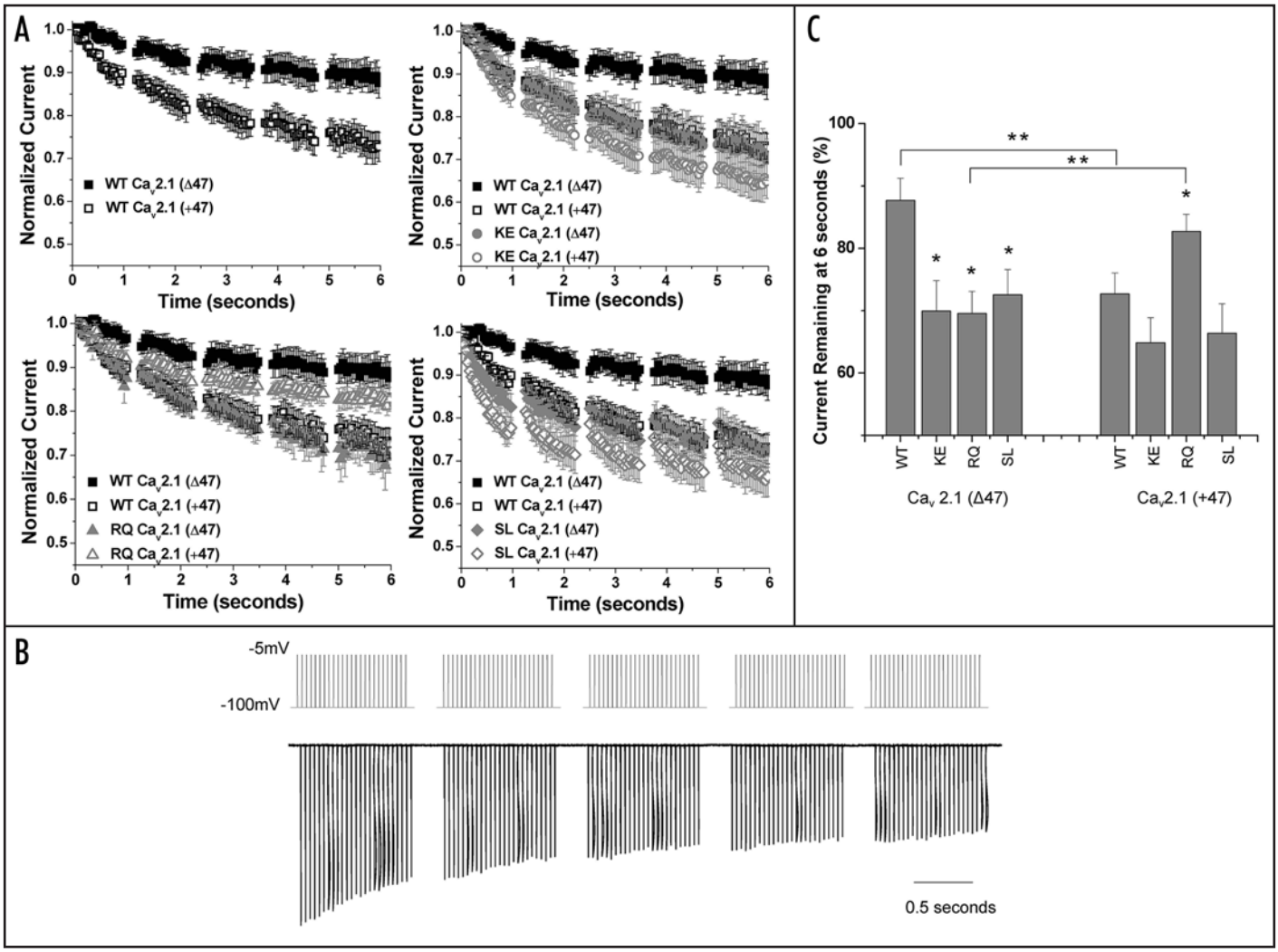

Figure 5. Wild-type and FHM-1 mutant $Ca_V2.1$ (Δ47) and $Ca_V2.1$ (+47) variants exhibit different current decay during bursts of depolarizations. (A) graphs show normalized current remaining vs. time after initial onset of depolarizations. Current decay was measured for wild-type (WT; black squares), FHM-1 mutant K1336E (KE; grey circles), R192Q (RQ; grey triangles) and S218L (SL; grey diamond) in both the short $Ca_V2.1$ (Δ47) (filled symbols) and long $Ca_V2.1$ (+47) (open symbols) C-terminus splice variants. (B) to investigate current decay during bursts of repetitive stimulations we used five bursts of 25 square pulses to -5 mV for 3.4 msec from a holding of -100 mV; bursts given at 290 msec intervals (3.5 Hz burst firing). Each burst contained 25 pulses at a rate of 25 Hz. Representative current trace indicated at bottom (capacitive transients were compensated using a P/4 protocol). (C) bar graph shows the percent of current remaining at the end of 6 seconds for each clone. Single asterisks and number signs indicate significant difference between mutant and wild-type of the same variant with p-values less than either 0.05 or 0.001 (one-way ANOVA), respectively. Double asterisks indicate significant difference between the $Ca_V2.1$ Δ47 and +47 variants containing the same sequence (i.e., WT or mutant) with p-value less than 0.05 (one-way ANOVA). Number of cells recorded for WT $Ca_V2.1$ (Δ47) (n = 8), WT $Ca_V2.1$ (+47) (n = 7), KE $Ca_V2.1$ (Δ47) (n = 8), KE $Ca_V2.1$ (+47) (n = 10), RQ $Ca_V2.1$ (Δ47) (n = 9), RQ $Ca_V2.1$ (+47) (n = 7), SL $Ca_V2.1$ (Δ47) (n =8), SL $Ca_V2.1$ (+47) (n = 8).

K1336E). Detailed single channel analyses would be required to fully explore this hypothesis.

Our findings provide the first suggestion for a potential role of P/Q-type channel alternative splicing in FHM-1 pathophysiology and raise the notion that even though $Ca_V2.1$ channels are widely expressed in the central and peripheral nervous systems, point mutations can have greater or lesser functional affects on specific splice variants. Although the mechanism of FHM-1 pathophysiology is not completely resolved, the current opinion is that the migraine usually initiates with aura due to CSD, which leads to headache pain through activation of the trigeminovascular pain pathway.[55,56] In this regard, specific $Ca_V2.1$ variants within the cortex may have important roles in the onset of migraine attacks.

We show that the $Ca_V2.1$ (Δ47) and $Ca_V2.1$ (+47) variants are both expressed in whole human cortex (Fig. 1B), and that the three FHM-1 mutations all cause a greater hyperpolarizing shift in the voltage-dependence of activation in $Ca_V2.1$ (Δ47) channels relative to that for $Ca_V2.1$ (+47) variant channels. A hyperpolarizing shift in P/Q-type channel activation has been suggested as an underlying mechanism of increased susceptibility to CSD and the initiation

of migraine.[22,57] CSD begins within small domains of the cortex and propagates outward from a focal point. Our data supports the notion that $Ca_V2.1$ splice variants with greater sensitivity to hyperpolarizing shifts in the voltage-dependence of activation (e.g., $Ca_V2.1$ (Δ47), could result in cortical regions with greater susceptibility to CSD and migraine initiation. Conversely, the effects of FHM-1 mutations on other $Ca_V2.1$ splice variants (e.g., $Ca_V2.1$ (+47)), expressed elsewhere in the cortex or other brain regions may be below the threshold to initiate CSD and/or other pathological effects. Future exploration of the exact regional and cellular distributions of these and other $Ca_V2.1$ splice variants within the cortex and throughout the human brain using in situ hybridization and/or RT-PCR analyses will be necessary to fully understand the role of $Ca_V2.1$ splice variants in FHM-1 pathology.

Our results examining tonic and burst firing patterns also suggests the possibility of differential effects of FHM-1 mutations on P/Q-type channel splice variants under different firing conditions. This is most clearly seen with the S218L mutation in the $Ca_V2.1$ (+47) variant; during tonic depolarization current decay is significantly faster relative to WT, yet during burst firing the S218L $Ca_V2.1$ (+47) variant has similar current decay to WT channels after five bursts, likely due to rapid recovery from inactivation (see Figs. 4 and 5). On the other hand, in $Ca_V2.1$ (Δ47) variant channels the S218L mutation has significant effects on current decay under both tonic and burst firing conditions. Interestingly, certain initiating factors of FHM-1 attacks such as emotional stress[14] are known to alter neuronal firing patterns in the brain.[58,59] Although the exact firing conditions directly associated with precipitating factors of migraine are unknown, the episodic nature of the FHM-1 phenotype may in part be associated with changes in neuronal firing pattern and/or frequency that could be relevant to specific $Ca_V2.1$ splice variants expressed in localized brain regions.

It is likely that there exists a complex relationship between channel missense mutations and disease mechanism. While we show alternative splicing at a single $Ca_V2.1$ splice-site can determine the functional impact of FHM-1 mutations, we recognize that across the entire brain many additional factors are likely to be involved in ultimately defining disease pathophysiology. These likely include the expression of multiple splice P/Q-type variants with distinct combinations of alternative splicing as well as the interaction with different auxiliary subunits[27] and other structural and regulatory proteins. Nonetheless, our results demonstrate the relevance of alternative splicing as an important factor in considering underlying disease molecular mechanisms and also the need for a comprehensive understanding of the splice-variant profile of $Ca_V2.1$ channels across brain regions and developmental stages as they might relate to FHM-1 pathology.

While in the present report we show that individual FHM-1 mutations can have differential effects on the biophysical properties of the short and long P/Q-type channel splice variants, we predict this phenomenon is likely relevant to both other FHM-1 mutations and $Ca_V2.1$ variants and also to other types of Ca_V channels and calcium channelopathies.[61] Understanding the differential effects of channelopathy mutations on ion channel splice variants is likely to be important for interpreting results obtained in both heterologous and native systems, as well as for making inferences concerning disease mechanisms and phenotypes. Mutations in the $Ca_V1.1$ L-type channel are associated with hypokalemic periodic paralysis, the $Ca_V1.2$ L-type with Timothy syndrome, the $Ca_V1.4$ L-type with incomplete X-linked congenital stationary night blindness and X-linked cone-rod dystrophy, and the $Ca_V3.2$ T-type with idiopathic generalized epilepsy and autism spectrum disorder (reviewed in ref. 4). Similar to FHM-1, many of these disorders exhibit phenotypes with episodic and/or developmentally specific attributes localized to a subset of regions or tissues that express the respective channels, and like $Ca_V2.1$, these channels also undergo alternative splicing that generates functionally distinct channel variants (reviewed in refs. 6 and 7). The identification of specific Ca_V splice variants involved in disease pathophysiology may also provide the opportunity for targeted therapeutic approaches. For example, while the $Ca_V2.2$ N-type channels have a central role in nociceptive signalling, distinct $Ca_V2.2$ splice variants are involved in the transmission of specific types of pain and has led to new strategies for splice variant-specific targeting in pain therapy.[60]

Methods

Site-directed mutagenesis. Standard PCR-based in vitro mutagenesis was performed using the Pfu Turbo DNA Polymerase (Stratagene, La Jolla, CA), 10 mM dNTPs (Invitrogen) and paired forward and reverse mutagenesis primers.[44] The human $Ca_V2.1$ long (+47) (isoform 2) (NCBI accession number NM_023035.1) cloned in pcDNA 3.1 Zeo (+) was used as the source for the generation of the WT short human $Ca_V2.1$ (Δ47) (isoform 1) cDNA (the other known six splice sites are: Δ10A, 16+/17+, -VEA, -NP, EFa, 43+/44+). Paired forward and reverse primers were designed to adhere to the C-terminus of the $Ca_V2.1$ isoform 2 at the exon 46/47 boundary nucleotide number 6784 and removed the GGCAG pentanucleotide sequence creating the premature stop in exon 47 ($Ca_V2.1$ (Δ47)). Both $Ca_V2.1$ splice variant cDNAs were used in site-directed mutagenesis reactions to generate human $Ca_V2.1$ K1336E, R192Q and S218L mutants in the short and long variants; paired forward and reverse primers were designed to convert codon 1336 from AAA to GAA, codon 192 from CGG to CAG, and codon 218 from TCG to TTA. The integrity of all constructs generated through site-directed mutagenesis were verified by direct DNA sequencing.

Cell culture and transfection. Human embryonic kidney (HEK 293) cells were grown in standard Dulbecco's modified Eagle's medium supplemented with 10% fetal bovine serum (heat inactivated) and 50 U/ml penicillin-50ug/ml streptomycin. Cells were incubated at 37°C in a humidified incubator with 95% atmosphere and 5% CO_2 and grown to 8–15% confluency for transfection. HEK 293 cells were transiently transfected with either WT human $Ca_V2.1$ (Δ47) or $Ca_V2.1$ (+47), or mutant K1336E $Ca_V2.1$ (Δ47), R192Q $Ca_V2.1$ (Δ47), S218L $Ca_V2.1$ (Δ47) or K1336E $Ca_V2.1$ (+47), R192Q $Ca_V2.1$ (+47), S218L $Ca_V2.1$ (+47) in combination with calcium channel auxiliary subunits β_4, $\alpha_2\delta$-1, and the CD8 marker plasmid in a 1:1:1:0.25 molar ratio using Lipofectamine (Invitrogen, La Jolla, CA). To ensure accurate

comparisons, transfections were performed at the same time and electrophysiological recordings alternated within the same day for all channel types.

Electrophysiological recordings. On the second day after transfection, macroscopic Ba^{2+} currents where recorded at room temperature using the whole-cell patch-clamp technique.[45] The internal pipette solution used contained 105 mM CsCl, 25 mM TEACl, 1 mM $CaCl_2$, 11 mM EGTA, 10 mM HEPES and 5 mM ATP (pH 7.2 with CsOH); external: 5 mM $BaCl_2$, 1 mM $MgCl_2$, 10 mM HEPES, 40 mM TEACl, 10 mM glucose and 87.5 mM CsCl (pH 7.4 with TEAOH). Patch pipettes (borosilicate glass BF150-86-10; Sutter Instrument Company, Novato, CA) were made using a horizontal puller (P-87; Sutter Instruments Company) and fire polished using a microforge (Narishige, Tokyo, Japan), with resistances typically of 3 to 5 MΩ when containing internal solution. External solution bath was connected to ground with a 3 M KCl agar bridge. Whole cell currents were recorded and filtered at 2–5 kHz bandwidth using an Axopatch 200A amplifier monitored and stored on a personal computer running pClamp software package version 9. Sampling frequencies were between 2 and 10 kHz. Recordings were analyzed using Clampfit 9 and figures, fittings and statistics (ANOVA) were made using the software program Origin version 7.5 (OriginLab Corp., Northampton, MA). Data are represented as mean ± standard error (S.E.).

Recording protocols and data analysis. Current-voltage relationships were determined by measured currents obtained using a series of 90 millisecond depolarization pulses applied from a holding potential of -90 mV to membrane potentials from -50 mV to +45 mV, increasing by 5 mV increments. Current-voltage relationships were fitted, and IV curves generated, using a modified Boltzmann equation:

$$I = (Gmax*(V_m - E_r))/(1 + \exp((V_m - V_{50})/k))$$

where Gmax is the maximum slope conductance, Vm is the test potential, E_r is the extrapolated reversal potential, V_{50} is the half-activation potential, and k reflects the slope of the activation curve. Activation curves were constructed by calculating conductance from the IV curves and plotting the normalized conductance as a function of the membrane potential. The data were fit with the Boltzmann equation:

$$G/Gmax = A2 + (A1 - A2)/(1 + \exp((V_m - V_{50})/k))$$

where A1 is minimum normalized conductance, A2 is maximum normalized conductance, V_m is the test potential, V_{50} is the half-activation potential, and k reflects the slope of the activation curve (goodness of fit had R^2 values ≥ 0.998).

Voltage-dependence of inactivation was analyzed using depolarizations to 0 mV for 80 ms following 5 s prepulses ranging from -100 to +10 mV at 10mV increments (holding potential of -120 mV). Steady state inactivation curves were constructed by plotting the maximum normalized current during the test pulse as a function of the prepulse potential. The data were fit with the Boltzmann equation:

$$I/Imax = A2 + (A1 - A2)/ (1 + \exp((V_m - V_{50})/k))$$

where A1 is minimum normalized current, A2 is the maximum normalized current, Vm is the test potential, V_{50} is the half-inactivation potential, and k reflects the slope of the inactivation curve (goodness of fit had R^2 values ≥ 0.998).

The kinetics of activation (τ_{act}) were determined from currents obtained from the IV protocol. Current traces were fit with a standard single exponential equation: $I = A*\exp(-t/\tau)$, where A is the amplitude of the current, and τ is the time constant.

Recovery from inactivation was determined using a double-pulse protocol. The first depolarization was to 0 mV for 2 s (the prepulse), followed by a return to the holding potential of -100 mV for variable lengths between 10 ms and 7.5 s. At the end of the variable repolarization period, a second 0 mV (the test pulse) was given for 50 ms. The time interval between sweeps was a total of 1 minute to ensure maximum recovery between sweeps. All traces were normalized to the maximum current during the prepulse for each sweep. The peak current from the test pulse was plotted as a percentage of maximum prepulse current vs. repolarization time. Average traces were fit with either a single or double exponential equation (goodness of fit had R^2 values ≥0.998).

Current decay during a tonic depolarization was examined using a 25 Hz train of 25 square pulses from a holding of -100 mV to a depolarizing potential of -5 mV for 3.4 ms. Current decay curves were generated by plotting normalized maximum current during the test pulses as a function of the time of pulse onset. Current decay during bursts of depolarization was examined using square pulses to -5 mV for 3.4 msec from a holding of -100 mV. Five bursts were given with 290 msec intervals (3.5 burst firing). Each burst contained 25 pulses at a rate of 25 Hz. Current decay curves were generated by plotting normalized maximum current during the test pulses as a function of the time of pulse onset.

RT-PCR of $Ca_V2.1$ carboxyl-terminal region from human cortex RNA. Prior to reverse transcription, 1 ug total RNA from human cortex (Clontech; 636561) was treated with 1X DNase I reaction buffer and 1 unit DNase I (Invitrogen) in a final volume adjusted to 10 uL using sterile DEPC-treated H_2O. Following a 15-minute incubation period at room temperature, the reaction was inactivated by adding 1 uL of 25 mM EDTA and heating at 65°C for 10 minutes. cDNA synthesis was performed using Superscript II Reverse Transcriptase (Invitrogen) following manufacturer's instructions with slight modification. A ~1.1-Kb nucleotide fragment of the carboxyl end of the $Ca_V2.1$ channel was amplified from the human cortex cDNA using standard PCR. The reaction mixture consisted of 3% DMSO, 1X Phusion enzyme buffer, 0.4 pmol/uL of forward and reverse primers, 0.2 mM dNTPs, 1 uL of cortex cDNA, and 1 unit of Phusion enzyme in a final volume of 25 uL. The forward primer (5'GGC ACA TGG AGT CCG GAA CA 3') corresponds to nucleotide position 6130 and the reverse primer (5'GGT AGT AGC CAT GGT GCC3') to nucleotide position 7211 of the human $Ca_V2.1$ α_1 subunit (NCBI accession number NM_023035.1). The cycling profile included an initial activation step of 98°C for 30 s

followed by 30 cycles of 98°C for 30 s, 65°C for 30 s, 72°C for 2.5 minutes and a final extension period of 72°C for 10 minutes. As positive controls, the same PCR reaction was performed on human $Ca_V2.1$ (Δ47) and $Ca_V2.1$ (+47) cDNA plasmids to demonstrate unbiased amplification. PCR reactions using primers for tubulin were used to verify the success of RT reactions. As negative controls, identical PCR reactions without template and containing no RT were performed. To analyze individual $Ca_V2.1$ amplified carboxyl terminal transcripts, PCR products were ligated into pGEMT-Easy (Promega) and then transformed into competent XL-1 *E.coli* bacterial cells. Bacteria containing PCR inserts were identified by blue-white screening and collected and subject to $Ca_V2.1$ (Δ47) and $Ca_V2.1$ (+47) specific PCR reactions. The reverse primer (5'GGT AGT AGC CAT GGT GCC3') was used for both $Ca_V2.1$ (Δ47) and $Ca_V2.1$ (+47) specific PCR reactions. Forward primer (5'ATG GCG CAC CGG CAG TA3') and (5'CAT GGC GCA CCG GCA GGG3') were designed to specifically amplify $Ca_V2.1$ (Δ47) and $Ca_V2.1$ (+47), respectively. All PCR products were run on a 1% agarose gel. In determining the percentage of each variants, only colonies positive for $Ca_V2.1$ (Δ47) and negative for $Ca_V2.1$ (+47), and visa versa, were included and ambiguous results discarded. Direct DNA sequence determination of several representative clones confirmed both the veracity of the splice-variant specific PCR reactions and the identity of the cloned PCR products.

Acknowledgements

This work was funded by operating grant #10677 from the Canadian Institutes of Health Research (CIHR) and a Tier 1 Canada Research Chair in Biotechnology and Genomics-Neurobiology to Terrance P. Snutch, an operating grant from the National Ataxia Foundation and a salary award from the Vancouver Coastal Health Authority to Sian D. Spacey, graduate fellowships from the Michael Smith Foundation for Health Research to Paul J. Adams and Kirk J. Mulatz, and a doctoral fellowship from the Heart and Stroke Foundation of Canada to Laurence S. David. We thank Dr. David Parker and Luke Materek for providing the wild-type isoform 2 $Ca_V2.1$ human cDNA and Ms. Alexi Millman for protocol optimization.

References

1. Catterall WA. Structure and regulation of voltage-gated Ca^{2+} channels. Annu Rev Cell Dev Biol 2000; 16:521-55.
2. Ptacek LJ, Tawil R, Griggs RC, Engel AG, Layzer RB, Kwiecinski H, et al. Dihydropyridine receptor mutations cause hypokalemic periodic paralysis. Cell 1994; 77:863-8.
3. Fontaine B, Vale-Santos J, Jurkat-Rott K, Reboul J, Plassart E, Rime CS, et al. Mapping of the hypokalaemic periodic paralysis (HypoPP) locus to chromosome 1q31-32 in three European families. Nat Genet 1994; 6:267-72.
4. Adams PJ, Snutch TP. Calcium channelopathies: voltage-gated calcium channels. Subcell Biochem 2007; 45:215-51.
5. Emerick MC, Stein R, Kunze R, McNulty MM, Regan MR, Hanck DA, Agnew WS. Profiling the array of $Ca_V3.1$ variants from the human T-type calcium channel gene CACNA1G: alternative structures, developmental expression and biophysical variations. Proteins 2006; 64:320-42.
6. Lipscombe D, Castiglioni AJ. Alternative Splicing in Voltage Gated Calcium Channels. In: McDonough SI, ed. Calcium Channel Pharmacology: Kluwer Academic/Plenum Publishers 2004; 369-409.
7. Lipscombe D, Pan JQ, Gray AC. Functional diversity in neuronal voltage-gated calcium channels by alternative splicing of $Ca_V\alpha_1$. Mol Neurobiol 2002; 26:21-44.
8. Gray AC, Raingo J, Lipscombe D. Neuronal calcium channels: splicing for optimal performance. Cell Calcium 2007; 42:409-17.
9. Splawski I, Timothy KW, Sharpe LM, Decher N, Kumar P, Bloise R, et al. $Ca_V1.2$ calcium channel dysfunction causes a multisystem disorder including arrhythmia and autism. Cell 2004; 119:19-31.
10. Splawski I, Timothy KW, Decher N, Kumar P, Sachse FB, Beggs AH, et al. Severe arrhythmia disorder caused by cardiac L-type calcium channel mutations. Proc Natl Acad Sci USA 2005; 102:8089-96.
11. Graves TD, Imbrici P, Kors EE, Terwindt GM, Eunson LH, Frants RR, et al. Premature stop codons in a facilitating EF-hand splice variant of $Ca_V2.1$ cause episodic ataxia type 2. Neurobiol Dis 2008; 32:10-5.
12. Zhuchenko O, Bailey J, Bonnen P, Ashizawa T, Stockton DW, Amos C, et al. Autosomal dominant cerebellar ataxia (SCA6) associated with small polyglutamine expansions in the alpha 1A-voltage-dependent calcium channel. Nat Genet 1997; 15:62-9.
13. Thomsen LL, Eriksen MK, Roemer SF, Andersen I, Olesen J, Russell MB. A population-based study of familial hemiplegic migraine suggests revised diagnostic criteria. Brain 2002; 125:1379-91.
14. Ducros A, Denier C, Joutel A, Cecillon M, Lescoat C, Vahedi K, et al. The clinical spectrum of familial hemiplegic migraine associated with mutations in a neuronal calcium channel. N Engl J Med 2001; 345:17-24.
15. Ophoff RA, Terwindt GM, Vergouwe MN, van Eijk R, Oefner PJ, Hoffman SM, et al. Familial hemiplegic migraine and episodic ataxia type-2 are caused by mutations in the Ca^{2+} channel gene CACNL1A4. Cell 1996; 87:543-52.
16. Bourinet E, Soong TW, Sutton K, Slaymaker S, Mathews E, Monteil A, et al. Splicing of alpha 1A subunit gene generates phenotypic variants of P- and Q-type calcium channels. Nat Neurosci 1999; 2:407-15.
17. Starr TV, Prystay W, Snutch TP. Primary structure of a calcium channel that is highly expressed in the rat cerebellum. Proc Natl Acad Sci USA 1991; 88:5621-5.
18. Westenbroek RE, Sakurai T, Elliott EM, Hell JW, Starr TV, Snutch TP, Catterall WA. Immunochemical identification and subcellular distribution of the alpha 1A subunits of brain calcium channels. J Neurosci 1995; 15:6403-18.
19. Takahashi T, Momiyama A. Different types of calcium channels mediate central synaptic transmission. Nature 1993; 366:156-8.
20. Sutton KG, McRory JE, Guthrie H, Murphy TH, Snutch TP. P/Q-type calcium channels mediate the activity-dependent feedback of syntaxin-1A. Nature 1999; 401:800-4.
21. Hans M, Luvisetto S, Williams ME, Spagnolo M, Urrutia A, Tottene A, et al. Functional consequences of mutations in the human alpha1A calcium channel subunit linked to familial hemiplegic migraine. J Neurosci 1999; 19:1610-9.
22. van den Maagdenberg AM, Pietrobon D, Pizzorusso T, Kaja S, Broos LA, Cesetti T, et al. A Cacna1a knockin migraine mouse model with increased susceptibility to cortical spreading depression. Neuron 2004; 41:701-10.
23. Tottene A, Fellin T, Pagnutti S, Luvisetto S, Striessnig J, Fletcher C, Pietrobon D. Familial hemiplegic migraine mutations increase Ca^{2+} influx through single human $Ca_V2.1$ channels and decrease maximal $Ca_V2.1$ current density in neurons. Proc Natl Acad Sci USA 2002; 99:13284-9.
24. Tottene A, Pivotto F, Fellin T, Cesetti T, van den Maagdenberg AM, Pietrobon D. Specific kinetic alterations of human $Ca_V2.1$ calcium channels produced by mutation S218L causing familial hemiplegic migraine and delayed cerebral edema and coma after minor head trauma. J Biol Chem 2005; 280:17678-86.
25. Tottene ASM, Frants RR, Ferrari M, van den Maagdenberg AMJ, Pietrobon D. Gain-Of-Function Of $Ca_V2.1$ Calcium Channels Leads To Increased Excitatory Synaptic Transmission In Microcultures Of Cortical Neurons From Cacna1a Knock-In Mice With The R192Q Familial Hemiplegic Migraine Mutation. Abstract Viewer/Itinerary Planner Washington, DC: Society for Neuroscience 2005; Online 2005.
26. Cao YQ, Tsien RW. Effects of familial hemiplegic migraine type 1 mutations on neuronal P/Q-type Ca^{2+} channel activity and inhibitory synaptic transmission. Proc Natl Acad Sci USA 2005; 102:2590-5.
27. Mullner C, Broos LA, van den Maagdenberg AM, Striessnig J. Familial hemiplegic migraine type 1 mutations K1336E, W1684R and V1696I alter $Ca_V2.1$ Ca^{2+} channel gating: evidence for beta-subunit isoform-specific effects. J Biol Chem 2004; 279:51844-50.
28. Kraus RL, Sinnegger MJ, Koschak A, Glossmann H, Stenirri S, Carrera P, Striessnig J. Three new familial hemiplegic migraine mutants affect P/Q-type Ca^{2+} channel kinetics. J Biol Chem 2000; 275:9239-43.
29. Melliti K, Grabner M, Seabrook GR. The familial hemiplegic migraine mutation R192Q reduces G-protein-mediated inhibition of P/Q-type ($Ca_V2.1$) calcium channels expressed in human embryonic kidney cells. J Physiol 2003; 546:337-47.
30. Gherardini LVDMA, Van De Ven RCG, Ferrari MD, Frants RR, Pietrobon D, Pizzorusso T. Increased susceptibility to cortical spreading depression in knockin mice carrying the S218L mutation of human $Ca_V2.1$ calcium channels: a new model for in vivo study of familial hemiplegic migraine type 1 (FHM1). Poster: Federation of European Neuroscience Societies Forum, Vienna Austria 2006.
31. Kraus RL, Sinnegger MJ, Glossmann H, Hering S, Striessnig J. Familial hemiplegic migraine mutations change alpha1A Ca^{2+} channel kinetics. J Biol Chem 1998; 273:5586-90.

32. Soong TW, DeMaria CD, Alvania RS, Zweifel LS, Liang MC, Mittman S, et al. Systematic identification of splice variants in human P/Q-type channel alpha1(2.1) subunits: implications for current density and Ca^{2+}-dependent inactivation. J Neurosci 2002; 22:10142-52.
33. Chang SY, Yong TF, Yu CY, Liang MC, Pletnikova O, Troncoso J, et al. Age and gender-dependent alternative splicing of P/Q-type calcium channel EF-hand. Neuroscience 2007; 145:1026-36.
34. Timmermann DB, Westenbroek RE, Schousboe A, Catterall WA. Distribution of high-voltage-activated calcium channels in cultured gamma-aminobutyric acidergic neurons from mouse cerebral cortex. J Neurosci Res 2002; 67:48-61.
35. Chaudhuri D, Chang SY, DeMaria CD, Alvania RS, Soong TW, Yue DT. Alternative splicing as a molecular switch for Ca^{2+}/calmodulin-dependent facilitation of P/Q-type Ca^{2+} channels. J Neurosci 2004; 24:6334-42.
36. Krovetz HS, Helton TD, Crews AL, Horne WA. C-Terminal alternative splicing changes the gating properties of a human spinal cord calcium channel alpha 1A subunit. J Neurosci 2000; 20:7564-70.
37. Restituito S, Thompson RM, Eliet J, Raike RS, Riedl M, Charnet P, Gomez CM. The polyglutamine expansion in spinocerebellar ataxia type 6 causes a β subunit-specific enhanced activation of P/Q-type calcium channels in *Xenopus* oocytes. J Neurosci 2000; 20:6394-403.
38. Maximov A, Sudhof TC, Bezprozvanny I. Association of neuronal calcium channels with modular adaptor proteins. J Biol Chem 1999; 274:24453-6.
39. Mori Y, Friedrich T, Kim MS, Mikami A, Nakai J, Ruth P, et al. Primary structure and functional expression from complementary DNA of a brain calcium channel. Nature 1991; 350:398-402.
40. Hans M, Urrutia A, Deal C, Brust PF, Stauderman K, Ellis SB, et al. Structural elements in domain IV that influence biophysical and pharmacological properties of human alpha1A-containing high-voltage-activated calcium channels. Biophys J 1999; 76:1384-400.
41. Fitzsimons RB, Wolfenden WH. Migraine coma. Meningitic migraine with cerebral oedema associated with a new form of autosomal dominant cerebellar ataxia. Brain 1985; 108:555-77.
42. Kors EE, Terwindt GM, Vermeulen FL, Fitzsimons RB, Jardine PE, Heywood P, et al. Delayed cerebral edema and fatal coma after minor head trauma: role of the CACNA1A calcium channel subunit gene and relationship with familial hemiplegic migraine. Ann Neurol 2001; 49:753-60.
43. Chan YC, Burgunder JM, Wilder-Smith E, Chew SE, Lam-Mok-Sing KM, Sharma V, Ong BK. Electroencephalographic changes and seizures in familial hemiplegic migraine patients with the CACNA1A gene S218L mutation. J Clin Neurosci 2008; 15:891-4.
44. Zoller MJ, Smith M. Oligonucleotide-directed mutagenesis: a simple method using two oligonucleotide primers and a single-stranded DNA template. DNA 1984; 3:479-88.
45. Hamill OP, Marty A, Neher E, Sakmann B, Sigworth FJ. Improved patch-clamp techniques for high-resolution current recording from cells and cell-free membrane patches. Pflugers Arch 1981; 391:85-100.
46. Weiss N, Sandoval A, Felix R, Van den Maagdenberg A, De Waard M. The S218L familial hemiplegic migraine mutation promotes deinhibition of $Ca_V2.1$ calcium channels during direct G-protein regulation. Pflugers Arch 2008; 457:315-26.
47. Womack M, Khodakhah K. Active contribution of dendrites to the tonic and trimodal patterns of activity in cerebellar Purkinje neurons. J Neurosci 2002; 22:10603-12.
48. Fernandez FR, Engbers JD, Turner RW. Firing dynamics of cerebellar purkinje cells. J Neurophysiol 2007; 98:278-94.
49. Shin SL, Rotter S, Aertsen A, De Schutter E. Stochastic description of complex and simple spike firing in cerebellar Purkinje cells. Eur J Neurosci 2007; 25:785-94.
50. McCormick DA, Connors BW, Lighthall JW, Prince DA. Comparative electrophysiology of pyramidal and sparsely spiny stellate neurons of the neocortex. J Neurophysiol 1985; 54:782-806.
51. Brumberg JC. Firing pattern modulation by oscillatory input in supragranular pyramidal neurons. Neuroscience 2002; 114:239-46.
52. Fellin T, Luvisetto S, Spagnolo M, Pietrobon D. Modal gating of human $Ca_V2.1$ (P/Q-type) calcium channels: II. The b mode and reversible uncoupling of inactivation. J Gen Physiol 2004; 124:463-74.
53. Luvisetto S, Fellin T, Spagnolo M, Hivert B, Brust PF, Harpold MM, et al. Modal gating of human $Ca_V2.1$ (P/Q-type) calcium channels: I. The slow and the fast gating modes and their modulation by beta subunits. J Gen Physiol 2004; 124:445-61.
54. Chaudhuri D, Issa JB, Yue DT. Elementary mechanisms producing facilitation of $Ca_V2.1$ (P/Q-type) channels. J Gen Physiol 2007; 129:385-401.
55. Bolay H, Reuter U, Dunn AK, Huang Z, Boas DA, Moskowitz MA. Intrinsic brain activity triggers trigeminal meningeal afferents in a migraine model. Nat Med 2002; 8:136-42.
56. Pietrobon D. Migraine: new molecular mechanisms. Neuroscientist 2005; 11:373-86.
57. Pietrobon D. Familial hemiplegic migraine. Neurotherapeutics 2007; 4:274-84.
58. Weiss JM, Simson PE. Neurochemical and electrophysiological events underlying stress-induced depression in an animal model. Adv Exp Med Biol 1988; 245:425-40.
59. McEwen BS. Physiology and neurobiology of stress and adaptation: central role of the brain. Physiol Rev 2007; 87:873-904.
60. Altier C, Dale CS, Kisilevsky AE, Chapman K, Castiglioni AJ, Matthews EA, et al. Differential role of N-type calcium channel splice isoforms in pain. J Neurosci 2007; 27:6363-73.
61. Powell KL, Cain SM, Ng C, Sirdesai S, David LS, Kyi M, Garcia E, Tyson JR, Reid CA, Bahlo M, Foote SJ, Snutch TP, O'Brien TJ. A $Ca_V3.2$ T-type calcium channel point mutation has splice-variant-specific effects on function and segregates with seizure expression in a polygenic rat model of absence epilepsy. J Neurosci 2009; 29:371-80.